

Scanning probe-induced thermoelectrics in a quantum point contact

Cite as: Appl. Phys. Lett. **119**, 043101 (2021); doi: [10.1063/5.0059220](https://doi.org/10.1063/5.0059220)

Submitted: 7 June 2021 · Accepted: 13 July 2021 ·

Published Online: 26 July 2021



View Online



Export Citation



CrossMark

Geneviève Fleury,^{1,a)}  Cosimo Gorini,¹  and Rafael Sánchez² 

AFFILIATIONS

¹Université Paris-Saclay, CEA, CNRS, SPEC, 91191 Gif-sur-Yvette, France

²Departamento de Física Teórica de la Materia Condensada, Condensed Matter Physics Center (IFIMAC) and Instituto Nicolás Cabrera, Universidad Autónoma de Madrid, 28049 Madrid, Spain

^{a)} Author to whom correspondence should be addressed: genevieve.fleury@cea.fr

ABSTRACT

We study three-terminal thermoelectric transport in a two-dimensional Quantum Point Contact (QPC) connected to left and right electronic reservoirs, as well as a third one represented by a scanning probe tip. The latter acts as a voltage probe exchanging heat with the system but no charges on average. The thermoelectric coefficients are calculated numerically within the Landauer–Büttiker formalism in the low-temperature and linear response regimes. We find tip-induced oscillations of the local and non-local thermopowers and study their dependence on the QPC opening. If the latter is tuned on a conductance plateau, the system behaves as a perfect thermoelectric diode: for some tip positions, the charge current through the QPC, driven by a local Seebeck effect, can flow in one direction only.

Published under an exclusive license by AIP Publishing. <https://doi.org/10.1063/5.0059220>

Progress in scanning probe techniques offers new opportunities for gaining understanding of energy transfers at the nanoscale. A major breakthrough was recently achieved in the field with the realization of high-resolution scanning probe thermometers,^{1,2} which allow mapping dissipation in quantum devices. Subsequently, this possibility of measuring local temperature on the nanoscale was leveraged to image the Peltier effect in graphene nanoconstrictions³ and nanowire heterostructures.⁴ Spatially resolved images of the Seebeck effect were measured by engineering local heaters with scanning tunneling⁵ or thermal^{3,4} microscopes, focused laser⁶ or electron⁷ beams, or Joule-heated nanowires.⁸ Contrary to conventional (longitudinal) thermoelectric measurements that are performed across two terminals, such experiments involve a third terminal (e.g., the tip of the microscope) and give access to non-local thermoelectric effects.

Three-terminal thermoelectrics has attracted growing interest for a decade,⁹ leading recently to experimental implementations.^{3–6,8,10–14} The prototypical system in this context consists of a central scattering region attached to two (say left and right) electronic reservoirs and to a third one with which only heat can be exchanged. The third terminal may be a bosonic reservoir,^{14–20} or a reservoir of electrons^{10–12,21} capacitively coupled to the scattering region. The essentials of such systems can be captured by a simplified model, where the third reservoir acts as a voltage probe, i.e., an electronic reservoir whose electrochemical potential floats so as to inject heat but no charge (on average) into the

system.²² The voltage probe model²³ is routinely employed to treat inelastic effects in mesoscopic systems.^{24–27} It has also been extensively used in the context of three-terminal thermoelectricity.^{28–31}

In this paper, we propose non-local and coherent thermoelectric manipulations in a two-dimensional quantum point contact (QPC) via the tip of a scanning tunneling microscope. The tip acts as a floating third terminal—a movable local voltage probe—perturbing the phase-coherent electronic propagation through the conductor in a controlled way.

QPCs are prototypical mesoscopic systems, whose two-terminal thermoelectric response was the subject of numerous theoretical^{32–40} and experimental^{40–45} works. In particular, the local thermopower of a QPC was recently⁴⁴ imaged by scanning gate microscopy (SGM) at low temperature (25 mK). In the present paper, the presence of the floating tip turns the basic QPC setup into the three-terminal device sketched in Fig. 1. We numerically study the local (longitudinal) and non-local thermoelectric response of the device, for different values of the intrinsic QPC transmission. The response is characterized by two fundamental features: (i) a charge current through the QPC can be induced by a non-local Seebeck effect, i.e., when the probe is heated, even in configurations where the QPC has no intrinsic thermoelectric response of its own; (ii) the probe can rectify a charge current driven by the local Seebeck effect, i.e., by heating the left (or right) terminal. We emphasize that both features are extrinsic, non-local and quantum interference-driven, as they require a third terminal and phase-coherent electronic propagation.

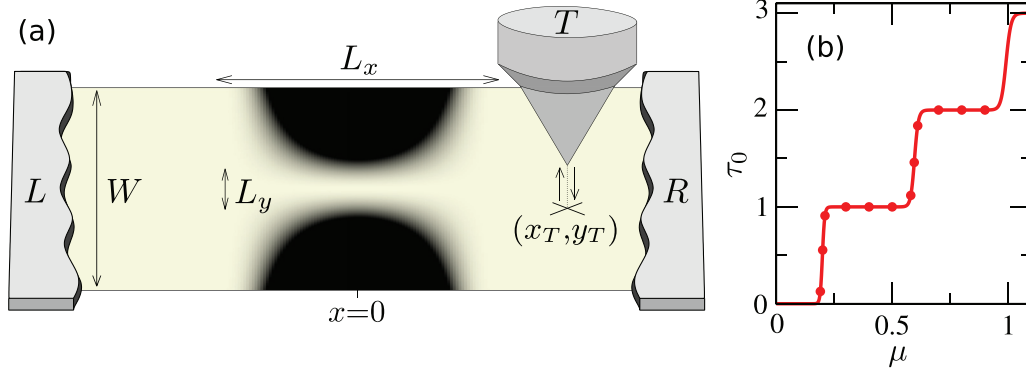


FIG. 1. (a) Sketch of our system. A ribbon of width W is attached to two left (L) and right (R) electronic reservoirs. The onsite confining potential $V_{qpc}(x, y)$ of characteristic length L_x and spatial opening L_y is shown in grayscale. A scanning tip at position (x_T, y_T) is attached to a third electronic reservoir (T). (b) QPC transmission τ_0 without tip, as a function of μ , in the limit of large W . The red dots indicate the values of μ considered in the top panels of Fig. 2.

Our model is as follows. We first introduce a translation-invariant ribbon of width W discretized on a square lattice (with lattice parameter a) and modeling the two-dimensional electron gas (2DEG) in the limit of large W . Its tight-binding Hamiltonian reads

$$H_{2DEG} = -t \sum_{\langle i,j \rangle} c_i^\dagger c_j + 4t \sum_i c_i^\dagger c_i, \quad (1)$$

where c_i^\dagger creates a (spinless) electron on site i at position $r_i = (x_i, y_i)$, the sum $\sum_{\langle i,j \rangle}$ is restricted to nearest neighbors, and t is the hopping parameter. The uniform potential $4t$ in Eq. (1) is included to set the bottom of the ribbon conduction band at zero energy. We model the QPC with a smooth (symmetric) confining onsite potential V_{qpc} defined by

$$V_{qpc}(x, y) = \left(\frac{y}{L_y}\right)^2 \left[1 - 3\left(\frac{2x}{L_x}\right)^2 + 2\left|\frac{2x}{L_x}\right|^3\right]^2, \quad (2)$$

if $|x| < L_x/2$ and $V_{qpc}(x, y) = 0$ elsewhere [L_x and L_y controlling, respectively, the length and the width of the QPC, as illustrated in Fig. 1(a)]. This defines the QPC Hamiltonian $H_{QPC} = \sum_i V_{qpc}(r_i) c_i^\dagger c_i$. Finally, the tip is modeled as a semi-infinite one-dimensional chain (with lattice parameter a) directed along the axis $z > 0$ perpendicular to the 2DEG. Its Hamiltonian reads

$$H_{tip} = -t \sum_{\langle i,j \rangle} c_i^\dagger c_j + 2t \sum_i c_i^\dagger c_i, \quad (3)$$

where c_i and c_i^\dagger now operate along $z > 0$. The site A at the extremity of the tip [of coordinates (x_T, y_T, a)] is coupled with the hopping term t_T to a single site B of the 2DEG [located at $(x_T, y_T, 0)$] below the tip. We denote by $H_c = -t_T c_A^\dagger c_B + \text{h.c.}$ the tunneling Hamiltonian between the tip and the ribbon.

In the following, we investigate three-terminal thermoelectric transport through the system defined by the Hamiltonian $H = H_{2DEG} + H_{QPC} + H_{tip} + H_c$. The three electronic reservoirs L , R , and T are formally attached, respectively, at the left and right extremities of the ribbon and at the end of the tip. They are kept at temperatures θ_α and electrochemical potentials μ_α ($\alpha = L, R$, or T). Within the Landauer-Büttiker formalism, the average charge (I_α^e) and heat (I_α^h)

currents flowing from the reservoir α to the scattering region are given by

$$I_\alpha^e = \frac{e}{h} \sum_{\beta \neq \alpha} \int dE \tau_{\alpha\beta}(E) [f_\alpha(E) - f_\beta(E)] \quad (4a)$$

$$I_\alpha^h = \frac{1}{h} \sum_{\beta \neq \alpha} \int dE (E - \mu_\alpha) \tau_{\alpha\beta}(E) [f_\alpha(E) - f_\beta(E)], \quad (4b)$$

where the sum runs over all reservoirs $\beta \neq \alpha$, $f_\alpha(E) = \{1 + \exp[(E - \mu_\alpha)/k_B \theta_\alpha]\}^{-1}$ is the Fermi-Dirac distribution, e is the electron charge, h and k_B are the Planck and Boltzmann constants, and $\tau_{\alpha\beta}(E)$ is the probability for an electron to be transmitted from β to α at energy E . Hereafter, we take the right reservoir as the reference and set $\mu_R = \mu$, $\theta_R = \theta$. We define $\Delta\mu_\alpha = \mu_\alpha - \mu$, $\Delta\theta_\alpha = \theta_\alpha - \theta$ for $\alpha = L$ and T , and assume that $\Delta\mu_\alpha$ and $\Delta\theta_\alpha$ are small enough so as to be in the linear response regime. By expanding the dimensionless currents $\bar{I}_\alpha^e = I_\alpha^e/(ek_B\theta/h)$ and $\bar{I}_\alpha^h = I_\alpha^h/(k_B^2\theta^2/h)$ to the first order in $\Delta\mu_\alpha/k_B\theta$ and $\Delta\theta_\alpha/\theta$, one obtains (for $\sigma = e, h$)

$$\bar{I}_\alpha^\sigma = \sum_{\beta=L,T} \left(L_{\alpha\beta}^{\sigma e} \frac{\Delta\mu_\beta}{k_B\theta} + L_{\alpha\beta}^{\sigma h} \frac{\Delta\theta_\beta}{\theta} \right), \quad (5)$$

in terms of the Onsager coefficients $L_{\alpha\beta}^{\sigma\sigma'}$. Time reversal symmetry implies $L_{\alpha\beta}^{\sigma\sigma'} = L_{\beta\alpha}^{\sigma'\sigma}$ and in the low temperature limit ($\theta \rightarrow 0$, to leading order in the Sommerfeld expansion),⁹

$$L_{\alpha\beta}^{ee} = -\tau_{\alpha\beta}(E = \mu) \quad \text{if } \alpha \neq \beta, \quad (6a)$$

$$L_{\alpha\beta}^{hh} = -\frac{\pi^2}{3} \tau_{\alpha\beta}(E = \mu) \quad \text{if } \alpha \neq \beta, \quad (6b)$$

$$L_{\alpha\beta}^{eh} = L_{\alpha\beta}^{he} = -\frac{\pi^2}{3} k_B \theta \partial_E \tau_{\alpha\beta}(E = \mu) \quad \text{if } \alpha \neq \beta, \quad (6c)$$

$$L_{\alpha\alpha}^{\sigma\sigma'} = -\sum_{\beta \neq \alpha} L_{\alpha\beta}^{\sigma\sigma'}. \quad (6d)$$

In Eq. (6d), the sum runs over all reservoirs $\beta \neq \alpha$ including R . Note also that Eq. (6d) resulting from charge and energy conservation is not restricted to low temperatures.

The transmission probabilities $\tau_{\alpha\beta}(E)$ and their derivatives $\partial_E \tau_{\alpha\beta}(E)$ are computed using the KWANT software.⁴⁶ Throughout

the paper, we take $L_x = 100 a_0$, $L_y = 5 a_0$, $a = 0.5 a_0$, and $t = t_0(a_0/a)^2$, the parameters $a_0 \equiv 1$ and $t_0 \equiv 1$ defining our space and energy units. The choice $a = 0.5 a_0$ allows us to capture the 2DEG continuum limit $a \rightarrow 0$ at low energies $0 < \mu \lesssim t_0$, yet keeping a tractable computation time. Finally, we introduce the notation τ_0 for the QPC transmission $\tau_{RL}(E = \mu)$ without tip ($t_T = 0$). With the chosen values of L_x and L_y , τ_0 shows well-defined quantized plateaus at $\tau_0 = 0, 1, 2, \dots$, see Fig. 1(b).

We assume in what follows that the tip acts as a voltage probe, i.e., $\Delta\mu_T$ adjusts in such a way that $I_T^e = 0$. Due to the Seebeck effect, a temperature bias $\Delta\theta_z$ generates a finite contribution to the charge current $I_L^e = -I_R^e$ through the 2DEG that can be canceled out by tuning the value of $\Delta\mu_L$. This value is determined by the thermopower²⁹ $S_{Lx} = -\Delta\mu_L/(e\Delta\theta_x)$ that has to be calculated under the conditions $I_L^e = I_T^e = 0$ and $\Delta\theta_{x'} = 0$ for $x' \neq x$. From Eq. (5), we get

$$S_{Lx} = \frac{k_B}{e} \frac{L_{TT}^{ee} L_{Lx}^{eh} - L_{LT}^{ee} L_{xT}^{eh}}{L_{LL}^{ee} L_{TT}^{ee} - L_{LT}^{ee} L_{LT}^{ee}}. \quad (7)$$

A non-local response appears when the left and right reservoirs are in equilibrium at the same θ ($\Delta\theta_L = 0$), while the tip reservoir is not ($\Delta\theta_T > 0$). At low temperatures, it gives

$$S_{LT} = \frac{\pi^2}{3} \frac{k_B}{e} k_B \theta \frac{\tau_{LT} \partial_E \tau_{TR} - \tau_{TR} \partial_E \tau_{LT}}{\tau_{LT} \tau_{TR} + \tau_{LR} \tau_{LT} + \tau_{LR} \tau_{TR}}, \quad (8)$$

where the transmissions and their derivatives are evaluated at μ . We study how S_{LT} depends on the position (x_T, y_T) of the tip, for different values of μ corresponding to different values of the QPC transmission τ_0 . We introduce $\tilde{S}_{LT} = S_{LT}/(\pi^2 k_B^2 \theta / 3e)$, which does not depend on the temperature θ [as long as the Sommerfeld expansion (8) is valid⁴⁷]. Our results are summarized in Fig. 2. Data of \tilde{S}_{LT} are shown near the QPC center where finite-width effects in W are negligible and the 2DEG limit is reached. This is illustrated by the superposition of dots (obtained with $W = 2000$) on lines (obtained with $W = 200$) in the top panels of Fig. 2. Note that when W is varied from 200 to 2000, the lattice spacing a is kept fixed while the ribbon width is increased. Moreover, $t_T = 0.1t$ was used in Fig. 2 but we have found that S_{LT}/t_T^2 is independent of t_T for small $t_T \lesssim 0.2t$ i.e., in the limit of a weakly coupled probe (see the supplementary material). Thus, the choice of the parameters θ , W , and t_T in Fig. 2 is irrelevant for the discussion hereafter as long as $\theta \rightarrow 0$, $W \gtrsim 200$ and $t_T \lesssim 0.2t$.

Let us now proceed with the analysis of the oscillations of $S_{LT}(x_T, y_T)$ shown in Fig. 2. They correspond to fringes of the interferometer formed by the QPC and the tip.⁴⁸ We find that $S_{LT}(-x_T, -y_T) = -S_{LT}(x_T, y_T)$ and $S_{LT}(x_T, -y_T) = S_{LT}(x_T, y_T)$. This is a direct consequence of the QPC reflection symmetries about the axis $x = 0$ and $y = 0$. In particular, $S_{LT} = 0$ when the tip is located at the QPC center $(0, 0)$ and preserves the QPC spatial symmetries. Moreover, the oscillations decay and eventually vanish when the tip is moved away from the QPC (i.e., $S_{LT} \rightarrow 0$ when $|x_T| \rightarrow \infty$, see the supplementary material for data at larger x_T). Another important result illustrated in Fig. 2 is the strong dependence on μ of the non-local thermopower. The amplitude of S_{LT} is much larger on the first QPC transmission step ($0 < \tau_0 < 1$, left column in Fig. 2) than on higher steps and plateaus ($\tau_0 \geq 1$).⁴⁹ The same behavior is known for the local thermopower $S_{LL}^0 = -\Delta\mu_L/(e\Delta\theta_L)|_{I_T^e=0}$ of a QPC without tip⁴⁰ and can be understood in the non-local configuration from the analysis of the different terms in Eq. (8) (see the supplementary material).

A striking difference between the QPC thermoelectric responses with or without tip appears when μ is tuned to one transmission plateau. Without tip, electron-hole symmetry around μ is preserved in the 2DEG; hence, $S_{LL}^0 = 0$ at low temperature: it is not possible to generate a finite charge current $I_L^e \neq 0$ through the QPC by Seebeck effect (i.e., with $\Delta\theta_L \neq 0$ but $\Delta\mu_L = 0$). On the contrary, in the presence of the tip there appear small but finite oscillations around zero of the non-local thermopower S_{LT} . This is because the tip breaks both electron-hole and left-right symmetries (see the second and fourth columns in Fig. 2 corresponding to $\tau_0(\mu) = 1$ and 2, respectively). Thus, a finite charge current $I_L^e \neq 0$ can be generated by non-local Seebeck effect (i.e., with $\Delta\theta_T \neq 0$ but $\Delta\theta_L = 0$ and $\Delta\mu_L = 0$) though the intrinsic thermoelectric response of the QPC vanishes.

Let us now discuss the colormaps of $S_{LT}(x_T, y_T)$ shown in the lower panels of Fig. 2. We find a non-trivial dependence on y_T which evolves when μ is varied: when the QPC is tuned to its first transmission step, $S_{LT}(x_T, y_T)$ has a single-lobe pattern around $y_T = 0$ [panel (e)] while two lobes appear near the QPC center on the first plateau [panel (f)], which evolve into two distinct branches on the second QPC step [panel (g)], and eventually a three-lobe pattern emerges on the second plateau [panel (h)]. The fact that the number of lobes depends on the opening of the QPC is reminiscent of the behavior of conductance fringes imaged by SGM,^{50,51} yet this dependence is

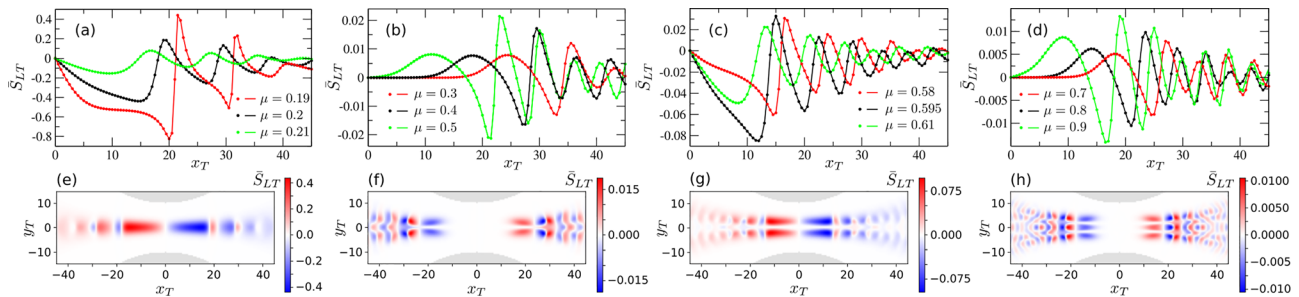


FIG. 2. Non-local thermopower \tilde{S}_{LT} in the low temperature limit, as a function of the tip position (x_T, y_T) , when the QPC is tuned to the first step (first column), first plateau (second column), second step (third column), and second plateau (last column) of conductance. (Top panels) $\tilde{S}_{LT}(x_T, y_T = 0)$ [(a) and (d)] and $\tilde{S}_{LT}(x_T, y_T = 3)$ [(b) and (c)] for different values of μ [indicated by red dots in Fig. 1(b)]. In all panels, data are shown for $W = 200$ (full lines) and $W = 2000$ (dots). (Bottom panels) $\tilde{S}_{LT}(x_T, y_T)$ for $\mu = 0.2$ (e), 0.4 (f), 0.595 (g), and 0.8 (h) with $W = 200$. Data on the grid are locally smoothed for better visibility. Regions where $V_{qpc}(x_T, y_T) \geq 4$ are shown in gray. In all panels, $t_T = 0.1t$.

different in both cases. Indeed, on the n -th QPC plateau, $n + 1$ lobes are visible in Figs. 2(f) and 2(h) while the SGM conductance interference fringes show n lobes.^{50,51}

We will now explore the longitudinal Seebeck effect and see how it can be leveraged in our system to implement a thermoelectric diode. We assume that the temperature bias is now finite in the left lead while $\Delta\theta_T = 0$. The tip still plays the role of a voltage probe, i.e., $\Delta\mu_T$ is determined by imposing $I_T^e = 0$. However, $I_T^h \neq 0$ in general. In that configuration, the linear response charge current flowing through the QPC reduces to

$$I_L^e = G_{LL} \left(\frac{\Delta\mu_L}{e} + S_{LL} \Delta\theta_L \right), \quad (9)$$

where the effective two-terminal conductance is given by

$$G_{LL} = \frac{e^2}{h} \left[L_{LL}^{ee} - \frac{(L_{LT}^{ee})^2}{L_{TT}^{ee}} \right], \quad (10)$$

and the local thermopower S_{LL} is obtained by taking $\alpha = L$ in Eq. (7). At low temperatures,

$$G_{LL} = \frac{e^2}{h} \left[\tau_{LR} + \frac{\tau_{LT}\tau_{TR}}{\tau_{LT} + \tau_{TR}} \right], \quad (11)$$

$$S_{LL} = \frac{\pi^2 k_B}{3e} \frac{\tau_{LT}\partial_E\tau_{LR} + \tau_{TR}\partial_E\tau_{LT} + \tau_{TR}\partial_E\tau_{LR}}{\tau_{LT}\tau_{TR} + \tau_{LR}\tau_{LT} + \tau_{LR}\tau_{TR}}. \quad (12)$$

The (dimensionless) transport coefficients $\bar{G}_{LL} = G_{LL}/(e^2/h)$ and $\bar{S}_{LL} = S_{LL}/(\pi^2 k_B^2 \theta / 3e)$ given by Eqs. (11) and (12) are plotted in Fig. 3 as functions of the tip position, for the same (four) values of μ considered in the lower panels of Fig. 2. As in Fig. 2, the 2DEG limit $W \rightarrow \infty$ is reached in the investigated region (near the QPC center). Also, defining \bar{G}_{LL}^0 and \bar{S}_{LL}^0 in the absence of the tip [$\bar{G}_{LL}^0 = \tau_0$ and $\bar{S}_{LL}^0 = (\partial_E\tau_0)/\tau_0$ at low temperature], we find that $(\bar{G}_{LL} - \bar{G}_{LL}^0)/t_T^2$ and $(\bar{S}_{LL} - \bar{S}_{LL}^0)/t_T^2$ are independent of t_T in the weak coupling limit ($t_T \lesssim 0.2t$), see the [supplementary material](#). When the QPC transmission is tuned on a step, \bar{G}_{LL} oscillates around \bar{G}_{LL}^0 [Figs. 3(a) and 3(c)]. On the plateaus, the tip-induced corrections to \bar{G}_{LL}^0 are of smaller

amplitude and always negative [Figs. 3(b) and 3(d)]. In both cases, $\bar{G}_{LL} \rightarrow \bar{G}_{LL}^0$ when $|x_T| \rightarrow \infty$. We notice that the behavior of G_{LL} described above is similar to the one of the two-terminal conductance of a QPC in a SGM configuration.^{50,51,53,54} Furthermore, we check that $\bar{G}_{LL}(x_T, y_T)$ is symmetric with respect to the axis $x_T = 0$. Indeed, when $(x_T, y_T) \rightarrow (-x_T, y_T)$, exchanging indices $L \leftrightarrow R$ in Eq. (11) and using $\tau_{\alpha\beta} = \tau_{\beta\alpha}$, \bar{G}_{LL} remains invariant. On the contrary, \bar{S}_{LL} is asymmetric with respect to $x_T = 0$. This can be understood from Eq. (12) likewise and stems from the fact that $\tau_{TR}\partial_E\tau_{LT} \neq \tau_{TL}\partial_E\tau_{RT}$ in general (see the [supplementary material](#) for more details). While the asymmetry is small when the QPC is tuned to a transmission step [Figs. 3(e) and 3(g)], it becomes prominent on the plateaus: then, the oscillations are strongly suppressed if the tip and the hot terminal are separated by the QPC [Figs. 3(f) and 3(h)]. In both cases, \bar{S}_{LL} oscillates around (and converges toward) the intrinsic QPC thermopower \bar{S}_{LL}^0 , as the tip is moved away from the QPC.

The asymmetry of the local thermopower patterns gives rise to current rectification effects. To make it clear, let us compare for a fixed position of the tip the (forward) current $I_{\rightarrow} = I_L^e$ when $\theta_L = \theta + \Delta\theta$ and $\theta_R = \theta_T = \theta$, to the (backward) current $I_{\leftarrow} = I_R^e$ when $\theta_R = \theta + \Delta\theta$ and $\theta_L = \theta_T = \theta$ (with otherwise $\mu_L = \mu_R = \mu$). We calculate $I_{\rightarrow} = S_{LL} G_{LL} \Delta\theta$ from Eqs. (11) and (12), while I_{\leftarrow} can be computed by reproducing the calculations from Eq. (4) with the left lead L (instead of R) as the reference. We check that $I_{\leftarrow}(x_T, y_T) = I_{\rightarrow}(-x_T, y_T)$ as imposed by the symmetry of the system. In general, $I_{\leftarrow}(x_T, y_T) \neq I_{\rightarrow}(x_T, y_T)$ [since $S_{LL}(x_T, y_T) \neq S_{LL}(-x_T, y_T)$]. To quantify the effect, we introduce the rectification parameter $\mathcal{R} = |I_{\rightarrow} - I_{\leftarrow}|/(|I_{\rightarrow}| + |I_{\leftarrow}|)$. Obviously, $\mathcal{R}(x_T, y_T) = \mathcal{R}(-x_T, y_T)$ and⁵⁵

$$\mathcal{R}(x_T, y_T) = \frac{|S_{LL}(x_T, y_T) - S_{LL}(-x_T, y_T)|}{|S_{LL}(x_T, y_T)| + |S_{LL}(-x_T, y_T)|}. \quad (13)$$

When the QPC is tuned to a transmission step, the asymmetry of S_{LL} is weak in comparison with the amplitude of S_{LL} (i.e., the numerator in Eq. (13) is negligible compared to the denominator) and, hence, \mathcal{R} is tiny [$\mathcal{R} \leq 0.002$ in Figs. 3(i) and 3(k)]. On the contrary, the strong asymmetry on the QPC plateaus leads to high rectification coefficients, $\mathcal{R} \approx 1$, and the system behaves as an efficient thermoelectric diode

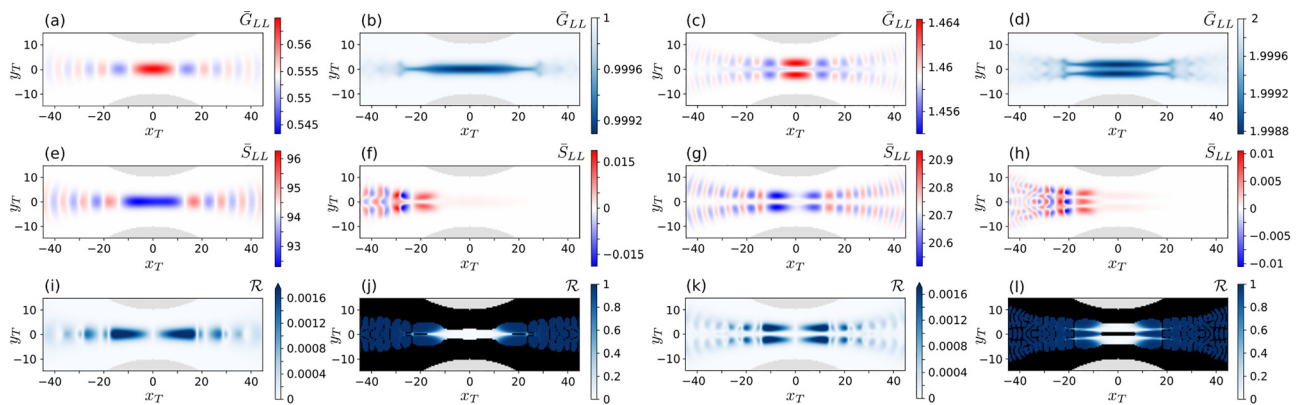


FIG. 3. Effective conductance \bar{G}_{LL} (first row), local thermopower \bar{S}_{LL} (second row), and rectification parameter \mathcal{R} (third row) in the low temperature limit, as a function of the tip position (x_T, y_T) , for $\mu = 0.2$ (first column), 0.4 (second column), 0.595 (third column), and 0.8 (last column). In the top and middle panels, the colormaps are chosen so as the white color corresponds to the values of \bar{G}_{LL} and \bar{S}_{LL} , respectively. In the bottom panels, data for \mathcal{R} with vanishingly small rectified currents ($(|I_{\rightarrow}| + |I_{\leftarrow}|)/(\pi^2 e k_B^2 \theta \Delta\theta / 3h) < 0.001$) are shown in black. In all panels, $W = 200$, $t_T = 0.1t$ and regions where $V_{qpc}(x, y) \geq 4$ are shown in gray.

[see Figs. 3(j) and 3(l)]. In other words, for $x_T > 0$ sufficiently far from the QPC, it is possible to generate a finite I_- by heating up the right reservoir, but not to generate a current I_- by heating up the left one (or conversely if $x_T < 0$). The rectification effect is perfect; however, the generated currents $\propto \bar{S}_{LL} \bar{G}_{LL}$ are small at the plateaus (compared to those generated at the steps), but in principle measurable. Note that other thermoelectric diodes were studied in the literature in various contexts.^{56–60} In our case, the optimal rectification effect exists within linear response and results from the simultaneous interference-induced broken left–right symmetry and the fact that the tip is allowed to exchange heat with the 2DEG (if $I_T^h = 0$ is imposed, $\mathcal{R} = 0$). We note also that a dual rectification effect of the heat current through the QPC is obtained if a voltage bias with respect to μ is applied between the left and right leads (instead of a temperature bias) and the tip plays the role of a thermal probe (with $I_T^h = 0$ and $\mu_T = \mu$) instead of a voltage probe. Within linear response and up to the lowest order of the Sommerfeld expansion (6), both rectification effects are controlled by the same rectification parameter given by Eqs. (13) and (12).

In conclusion, we studied low-temperature non-local thermoelectric effects in a QPC coupled to a scanning voltage probe, in linear response to small thermal/voltage biases. The probe is floating, i.e., it exchanges heat but no (average) charge with the 2DEG. However, it affects the thermoelectric response of the three-terminal device, by two main features. First, a finite non-local thermopower oscillates as a function of the probe position, even when the QPC is open on a conductance plateau, and thus, its intrinsic (without probe) low-temperature thermopower vanishes. The oscillations are signatures of the electronic interferometer formed by the QPC and the probe: when the latter is heated, it injects (neutral) electron-hole excitations into the 2DEG, which induce a net charge current through the QPC as the interferometer breaks both left–right and electron–hole symmetries. Second, the local thermopower oscillates as a function of the probe position as well, around its intrinsic value. When the QPC is open on a conductance plateau, such oscillations are visible if the tip is on the hot reservoir side, but quickly die out otherwise. This asymmetric quantum interference pattern leads to potentially perfect current rectification. Such a rectification is enabled by the presence of the tip, thus bypassing the fundamental limitations of standard (two-terminal) linear response theory.

Our results are proof-of-principle and concern small currents in a bare-bone QPC interferometer. We hope that they will motivate further (experimental) investigations of the thermoelectric response of nanostructures with scanning probe techniques.

See the [supplementary material](#) which shows additional data for various W and t_T , and additional plots of the transmissions $\tau_{\alpha\beta}$ and their derivatives $\partial_E \tau_{\alpha\beta}$ entering Eqs. (8) and (12). The effect of auxiliary fictitious probes playing the role of (invasive) local thermometers is also investigated.

G.F. thanks Rodolfo Jalabert and Dietmar Weinmann for useful discussions. R.S. acknowledges funding from the Ramón y Cajal Program RYC-2016-20778, and the Spanish Ministerio de Ciencia e Innovación via Grant No. PID2019-110125GB-I00 and through the “María de Maeztu” Programme for Units of Excellence in R&D No. CEX2018-000805-M. C.G. acknowledges stimulating discussions with the STHERQO members.

DATA AVAILABILITY

The data that support the findings of this study are available from the corresponding author upon reasonable request.

REFERENCES

- ¹F. Menges, P. Mensch, H. Schmid, H. Riel, A. Stemmer, and B. Gotsmann, “Temperature mapping of operating nanoscale devices by scanning probe thermometry,” *Nat. Commun.* **7**, 10874 (2016).
- ²D. Halbertal, J. Cuppens, M. B. Shalom, L. Embon, N. Shadmi, Y. Anahory, H. Naren, J. Sarkar, A. Uri, Y. Ronen, Y. Myasoedov, L. Levitov, E. Joselevich, A. K. Geim, and E. Zeldov, “Nanoscale thermal imaging of dissipation in quantum systems,” *Nature* **539**, 407 (2016).
- ³A. Harzheim, J. Spiege, C. Evangelii, E. McCann, V. Falko, Y. Sheng, J. H. Warner, G. A. D. Briggs, J. A. Mol, P. Gehring, and O. V. Kolosov, “Geometrically enhanced thermoelectric effects in graphene nanoconstrictions,” *Nano Lett.* **18**, 7719 (2018).
- ⁴N. Gächter, F. Könenmann, M. Sistani, M. G. Bartmann, M. Sousa, P. Staudinger, A. Lugstein, and B. Gotsmann, “Spatially resolved thermoelectric effects in operando semiconductor–metal nanowire heterostructures,” *Nanoscale* **12**, 20590 (2020).
- ⁵J. Park, G. He, R. M. Feenstra, and A.-P. Li, “Atomic-scale mapping of thermoelectric power on graphene: Role of defects and boundaries,” *Nano Lett.* **13**, 3269 (2013).
- ⁶P. Zolotavin, C. I. Evans, and D. Natelson, “Substantial local variation of the Seebeck coefficient in gold nanowires,” *Nanoscale* **9**, 9160 (2017).
- ⁷J. Fast, E. Barrigon, M. Kumar, Y. Chen, L. Samuelson, M. Borgström, A. Gustafsson, S. Limpert, A. Burke, and H. Linke, “Hot-carrier separation in heterostructure nanowires observed by electron-beam induced current,” *Nanotechnology* **31**, 394004 (2020).
- ⁸R. Mitra, M. R. Sahu, A. Sood, T. Taniguchi, K. Watanabe, H. Shtrikman, S. Mukerjee, A. K. Sood, and A. Das, “Anomalous thermopower oscillations graphene-InAs nanowire vertical heterostructures,” *arXiv:2009.08882* (2020).
- ⁹G. Benenti, G. Casati, K. Saito, and R. S. Whitney, “Fundamental aspects of steady-state conversion of heat to work at the nanoscale,” *Phys. Rep.* **694**, 1 (2017).
- ¹⁰B. Roche, P. Roulleau, T. Jullien, Y. Jompol, I. Farrer, D. A. Ritchie, and D. C. Glattli, “Harvesting dissipated energy with a mesoscopic ratchet,” *Nat. Commun.* **6**, 6738 (2015).
- ¹¹H. Thierschmann, R. Sánchez, B. Sothmann, F. Arnold, C. Heyn, W. Hansen, H. Buhmann, and L. W. Molenkamp, “Three-terminal energy harvester with coupled quantum dots,” *Nat. Nanotechnol.* **10**, 854 (2015).
- ¹²F. Hartmann, P. Pfeffer, S. Höfling, M. Kamp, and L. Worschech, “Voltage fluctuation to current converter with Coulomb-coupled quantum dots,” *Phys. Rev. Lett.* **114**, 146805 (2015).
- ¹³G. Jaliel, R. K. Puddy, R. Sánchez, A. N. Jordan, B. Sothmann, I. Farrer, J. P. Griffiths, D. A. Ritchie, and C. G. Smith, “Experimental realization of a quantum dot energy harvester,” *Phys. Rev. Lett.* **123**, 117701 (2019).
- ¹⁴S. Dorsch, A. Svilans, M. Josefsson, B. Goltzian, M. Kumar, C. Thelander, A. Wacker, and A. Burke, “Heat driven transport in serial double quantum dot devices,” *Nano Lett.* **21**, 988–994 (2021).
- ¹⁵B. Rutten, M. Esposito, and B. Cleuren, “Reaching optimal efficiencies using nanosized photoelectric devices,” *Phys. Rev. B* **80**, 235122 (2009).
- ¹⁶O. Entin-Wohlman, Y. Imry, and A. Aharony, “Three-terminal thermoelectric transport through a molecular junction,” *Phys. Rev. B* **82**, 115314 (2010).
- ¹⁷T. Ruokola and T. Ojanen, “Theory of single-electron heat engines coupled to electromagnetic environments,” *Phys. Rev. B* **86**, 035454 (2012).
- ¹⁸B. Sothmann and M. Büttiker, “Magnon-driven quantum-dot heat engine,” *Europhys. Lett.* **99**, 27001 (2012).
- ¹⁹J.-H. Jiang, O. Entin-Wohlman, and Y. Imry, “Thermoelectric three-terminal hopping transport through one-dimensional nanosystems,” *Phys. Rev. B* **85**, 075412 (2012).
- ²⁰R. Bosisio, G. Fleury, J.-L. Pichard, and C. Gorini, “Nanowire-based thermoelectric ratchet in the hopping regime,” *Phys. Rev. B* **93**, 165404 (2016).
- ²¹R. Sánchez and M. Büttiker, “Optimal energy quanta to current conversion,” *Phys. Rev. B* **83**, 085428 (2011).

- ²²A. N. Jordan, B. Sothmann, R. Sánchez, and M. Büttiker, "Powerful and efficient energy harvester with resonant-tunneling quantum dots," *Phys. Rev. B* **87**, 075312 (2013).
- ²³M. Büttiker, "Role of quantum coherence in series resistors," *Phys. Rev. B* **33**, 3020 (1986).
- ²⁴Y. Xing, Q.-F. Sun, and J. Wang, "Influence of dephasing on the quantum Hall effect and the spin Hall effect," *Phys. Rev. B* **77**, 115346 (2008).
- ²⁵P. Roulleau, F. Portier, P. Roche, A. Cavanna, G. Faini, U. Gennser, and D. Mailly, "Tuning decoherence with a voltage probe," *Phys. Rev. Lett.* **102**, 236802 (2009).
- ²⁶M. Kilgour and D. Segal, "Inelastic effects in molecular transport junctions: The probe technique at high bias," *J. Chem. Phys.* **144**, 124107 (2016).
- ²⁷Q. Ma, F. D. Parmentier, P. Roulleau, and G. Fleury, "Graphene $n-p$ junctions in the quantum Hall regime: Numerical study of incoherent scattering effects," *Phys. Rev. B* **97**, 205445 (2018).
- ²⁸D. Sánchez and L. Serra, "Thermoelectric transport of mesoscopic conductors coupled to voltage and thermal probes," *Phys. Rev. B* **84**, 201307 (2011).
- ²⁹F. Mazza, R. Bosisio, G. Benenti, V. Giovannetti, R. Fazio, and F. Taddei, "Thermoelectric efficiency of three-terminal quantum thermal machines," *New J. Phys.* **16**, 085001 (2014).
- ³⁰F. Mazza, S. Valentini, R. Bosisio, G. Benenti, V. Giovannetti, R. Fazio, and F. Taddei, "Separation of heat and charge currents for boosted thermoelectric conversion," *Phys. Rev. B* **91**, 245435 (2015).
- ³¹R. Sánchez, B. Sothmann, and A. N. Jordan, "Effect of incoherent scattering on three-terminal quantum Hall thermoelectrics," *Physica E* **75**, 86 (2016).
- ³²P. Streda, "Quantised thermopower of a channel in the ballistic regime," *J. Phys.: Condens. Matter* **1**, 1025–1027 (1989).
- ³³C. R. Proetto, "Thermopower oscillations of a quantum-point contact," *Phys. Rev. B* **44**, 9096 (1991).
- ³⁴M. A. Cipiloğlu, S. Turgut, and M. Tomak, "Nonlinear Seebeck and Peltier effects in quantum point contacts," *Phys. Status Solidi B* **241**, 2575 (2004).
- ³⁵A. M. Lunde and K. Flensberg, "On the Mott formula for the thermopower of non-interacting electrons in quantum point contacts," *J. Phys.: Condens. Matter* **17**, 3879 (2005).
- ³⁶A. Abbout, "Thermoelectric transport in quantum point contacts and chaotic cavities: Thermal effects and fluctuations," Ph.D. thesis (University Paris VI, 2011).
- ³⁷R. S. Whitney, "Nonlinear thermoelectricity in point contacts at pinch off: A catastrophe aids cooling," *Phys. Rev. B* **88**, 064302 (2013).
- ³⁸S. Pilgram, D. Sánchez, and R. López, "Quantum point contacts as heat engines," *Physica E* **74**, 447 (2015).
- ³⁹S. Kheradsoud, N. Dashti, M. Misiorny, P. P. Potts, J. Splettstoesser, and P. Samuelsson, "Power, efficiency and fluctuations in a quantum point contact as steady-state thermoelectric heat engine," *Entropy* **21**, 777 (2019).
- ⁴⁰H. van Houten, L. W. Molenkamp, C. W. J. Beenakker, and C. T. Foxon, "Thermo-electric properties of quantum point contacts," *Semicond. Sci. Technol.* **7**, B215 (1992).
- ⁴¹L. W. Molenkamp, T. Gravier, H. van Houten, O. J. A. Buijk, M. A. A. Mabeoone, and C. T. Foxon, "Peltier coefficient and thermal conductance of a quantum point contact," *Phys. Rev. Lett.* **68**, 3765 (1992).
- ⁴²A. S. Dzurak, C. G. Smith, L. Martin-Moreno, M. Pepper, D. A. Ritchie, G. A. C. Jones, and D. G. Hasko, "Thermopower of a one-dimensional ballistic constriction in the non-linear regime," *J. Phys.: Condens. Matter* **5**, 8055 (1993).
- ⁴³N. J. Appleyard, J. T. Nicholls, M. Y. Simmons, W. R. Tribe, and M. Pepper, "Thermometer for the 2D electron gas using 1D thermopower," *Phys. Rev. Lett.* **81**, 3491 (1998).
- ⁴⁴B. Brun, F. Martins, S. Faniel, A. Cavanna, C. Ulysse, A. Ouerghi, U. Gennser, D. Mailly, P. Simon, S. Huant, M. Sanquer, H. Sellier, V. Bayot, and B. Hackens, "Thermoelectric scanning-gate interferometry on a quantum point contact," *Phys. Rev. Appl.* **11**, 034069 (2019).
- ⁴⁵C. Yan, M. Pepper, P. See, I. Farrer, D. A. Ritchie, and J. Griffiths, "Thermoelectric property of a one dimensional channel in the presence of a transverse magnetic field," *Appl. Phys. Lett.* **115**, 202102 (2019).
- ⁴⁶C. W. Groth, M. Wimmer, A. R. Akhmerov, and X. Waintal, "Kwant: A software package for quantum transport," *New J. Phys.* **16**, 063065 (2014).
- ⁴⁷This is valid when $k_B\theta$ is much smaller than the typical energy scale ΔE associated to the oscillations of $\tau_{\alpha\beta}(E)$. While ΔE decreases with $|x_T|$, the oscillations of $\tau_{\alpha\beta}(E)$ are expected to average out at large $|x_T|$.
- ⁴⁸M. Büttiker, "Chemical potential oscillations near a barrier in the presence of transport," *Phys. Rev. B* **40**, 3409–3412 (1989).
- ⁴⁹Formally, $|S_{LT}|$ becomes even larger and larger when the QPC is gradually pinched off ($\tau_0 \rightarrow 0$) upon decreasing μ , but this regime is out of reach experimentally.
- ⁵⁰M. A. Topinka, B. J. LeRoy, S. E. J. Shaw, E. J. Heller, R. M. Westervelt, K. D. Maranowski, and A. C. Gossard, "Imaging coherent electron flow from a quantum point contact," *Science* **289**, 2323 (2000).
- ⁵¹C. Gorini, R. A. Jalabert, W. Szewc, S. Tomsovic, and D. Weinmann, "Theory of scanning gate microscopy," *Phys. Rev. B* **88**, 035406 (2013).
- ⁵²The convergence is not obvious in Figs. 3(b) and 3(d) limited to $|x_T| < 45$ but we have checked it by considering larger values of x_T (and of W to eliminate finite-size effects that arise away from the QPC).
- ⁵³M. P. Jura, M. A. Topinka, M. Grobis, L. N. Pfeiffer, K. W. West, and D. Goldhaber-Gordon, "Electron interferometer formed with a scanning probe tip and quantum point contact," *Phys. Rev. B* **80**, 041303 (2009).
- ⁵⁴R. A. Jalabert, W. Szewc, S. Tomsovic, and D. Weinmann, "What is measured in the scanning gate microscopy of a quantum point contact?," *Phys. Rev. Lett.* **105**, 166802 (2010).
- ⁵⁵Within linear response, \mathcal{R} can also be written as $\mathcal{R} = |S_{LT}|/(|S_{LL}| + |S_{LT} + S_{LL}|)$. With this formula, the discussion held after Eq. (13) can be rephrased as follows. On the QPC steps, $|S_{LL}| \gg |S_{LT}|$ and \mathcal{R} is tiny. On the QPC plateaus, there are some tip positions for which $S_{LL}(x_T, y_T) = 0$ and so $\mathcal{R} = 1$. In that case, $S_{LL}(-x_T, y_T) = -S_{LT}(-x_T, y_T)$ [compare Figs. 2(f)–3(f) and Figs. 2(h)–3(h)], hence $\mathcal{R}(-x_T, y_T) = 1$ too and we recover the expected symmetry law $\mathcal{R}(x_T, y_T) = \mathcal{R}(-x_T, y_T)$.
- ⁵⁶D. M.-T. Kuo and Y.-C. Chang, "Thermoelectric and thermal rectification properties of quantum dot junctions," *Phys. Rev. B* **81**, 205321 (2010).
- ⁵⁷J. Matthews, D. Sánchez, M. Larsson, and H. Linke, "Thermally driven ballistic rectifier," *Phys. Rev. B* **85**, 205309 (2012).
- ⁵⁸Z. H. Zhang, Y. S. Gui, L. Fu, X. L. Fan, J. W. Cao, D. S. Xue, P. P. Freitas, D. Houssameddine, S. Hemour, K. Wu, and C.-M. Hu, "Seebeck rectification enabled by intrinsic thermoelectrical coupling in magnetic tunneling junctions," *Phys. Rev. Lett.* **109**, 037206 (2012).
- ⁵⁹G. Rosselló, R. López, and R. Sánchez, "Dynamical Coulomb blockade of thermal transport," *Phys. Rev. B* **95**, 235404 (2017).
- ⁶⁰G. T. Craven, D. He, and A. Nitzan, "Electron-transfer-induced thermal and thermoelectric rectification," *Phys. Rev. Lett.* **121**, 247704 (2018).